

## Synthesis, characterization and DNA nuclease activity of oxo-peroxomolybdenum(VI) complexes

Shiv Shankar Paul, Md. Selim & Kalyan K. Mukherjea

To cite this article: Shiv Shankar Paul, Md. Selim & Kalyan K. Mukherjea (2017) Synthesis, characterization and DNA nuclease activity of oxo-peroxomolybdenum(VI) complexes, Journal of Coordination Chemistry, 70:10, 1739-1760, DOI: [10.1080/00958972.2017.1310378](https://doi.org/10.1080/00958972.2017.1310378)

To link to this article: <http://dx.doi.org/10.1080/00958972.2017.1310378>



Accepted author version posted online: 30 Mar 2017.  
Published online: 10 Apr 2017.



Submit your article to this journal [↗](#)



Article views: 18



View related articles [↗](#)



View Crossmark data [↗](#)



## Synthesis, characterization and DNA nuclease activity of oxo-peroxomolybdenum(VI) complexes

Shiv Shankar Paul, Md. Selim<sup>‡</sup> and Kalyan K. Mukherjea

Department of Chemistry, Jadavpur University, Kolkata, India

### ABSTRACT

The synthesis and structural characterization of two oxo-peroxo molybdenum(VI) complexes,  $[\text{Mo}(\text{O})(\text{O})_2(\text{PAA})]^-$  (**1**) and  $[\text{Mo}(\text{O})(\text{O})_2(\text{PAH})]^-$  (**2**), with phenylacetic acid (PAA) and 2-phenylacetyl-hydroxamic acid (PAHH) ligands have been accomplished. The coordination geometry of the oxo-peroxo molybdenum(VI) complexes is found to be pentagonal bipyramidal where, in both cases, the ligands are coordinated in bidentate fashion through oxygen atoms. The binding affinities of **1** and **2** with calf-thymus DNA (CT DNA) are determined using absorption spectroscopic measurements. The spectroscopic as well as cyclic voltammetric (CV) studies and viscosity measurements indicate that both complexes interact with CT DNA in the groove. The intrinsic binding constants are  $5.2 \times 10^4 \text{ M}^{-1}$  and  $7.3 \times 10^4 \text{ M}^{-1}$  for **1** and **2**, respectively, from UV–vis studies. Complexes **1** and **2** show nuclease activity with plasmid DNA in the presence of  $\text{H}_2\text{O}_2$ . Concentration-dependent nuclease study suggests that **2** possesses higher ability to cleave plasmid DNA compared to **1**. The experimental results of the binding of **1** and **2** with DNA are further supported by molecular docking studies.

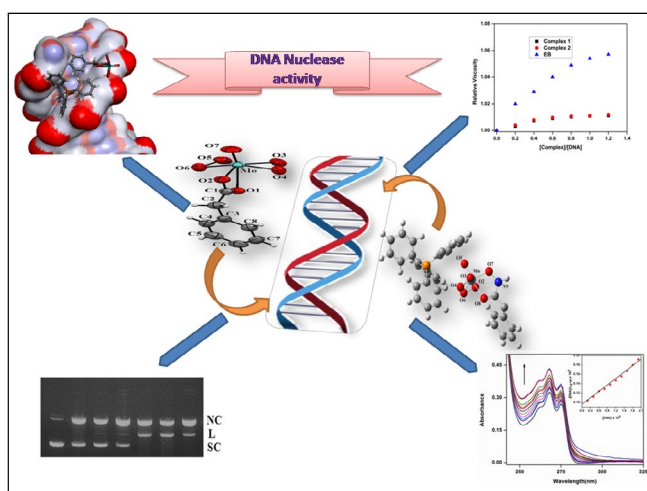
### ARTICLE HISTORY

Received 21 November 2016

Accepted 2 March 2017

### KEYWORDS

Oxo-diperoxo molybdenum(VI) complexes; single-crystal X-ray structure; DFT; DNA-binding study; DNA nuclease activity



**CONTACT** Kalyan K. Mukherjea  k\_mukherjea@yahoo.com

<sup>‡</sup> Present address: Department of Chemistry, Vivekananda College, Kolkata 700063, India.

## 1. Introduction

Small molecules that interact with DNA through recognition, binding, modifying, cleaving, or cross-linking have attracted wide attention in various fields of chemistry, biology, biotechnology, and medicine [1]. Like natural enzymes, artificial nucleases can hydrolyze DNA, and therefore these cleavage agents have found extensive applications in DNA manipulations and as potential chemotherapeutics [2]. Oxidative cleavage of DNA requires co-reactants to initiate and is mediated by reactive oxygen species (ROS) that cause other severe cytotoxic effects [3]. The phosphodiester bonds of DNA are exceptionally resistant to hydrolysis [4], so to overcome hydrolysis, natural nucleases such as restriction endonucleases and topoisomerases are very efficient catalysts, wherein, their activity is attributed to the involvement of active metal centers [5]. Artificial metallonucleases can be potentially used in gene regulation, mapping of protein and DNA-interactions, probing of DNA specific structures, and in cancer therapy [6]. Fe, Cu, Ni, Pt, Ru, Rh, V, Cr, Co, Mn, Os, and Pd complexes have been reported to mediate DNA-cleavage [7] in the presence of oxidants or reductants or without any assisting agents, whereas the role of molybdenum remained mostly unexplored as nuclease. Molybdenum is a unique 4d transition element in the periodic table due to its varied roles, and probably the most prominent use of this element is in the form of biocatalysts as found in the enzymatic reactions in several molybdoproteins in nature [8]. Investigation on the role of Mo as a biometal has become an area of research to understand the fascinating coordination and bioinorganic modeling chemistry of mononuclear molybdenum-containing enzymes. Oxo-peroxo and dioxo Mo(VI) complexes with polydentate nitrogen, sulfur, and oxygen ligands are considered valuable models for the active site of several Mo enzymes [9].

DNA has been known to be one of the conventional targets of chemotherapeutics in the management of human cancers [10]. Transition metal complexes are known to bind to DNA via both covalent and/or non-covalent interactions. In the case of covalent binding, a labile ligand of the complex can be replaced by a nitrogen base of DNA such as guanine N7, while the non-covalent DNA interactions include intercalative, electrostatic, and groove (surface) binding of a metal complex outside the DNA helix along the major or minor grooves [11]. The major and minor grooves of DNA act as a passage for molecular information required for DNA-interaction with other molecules since hydrogen bonding centers in bases are pointed into these grooves. Thus, small DNA-binders interact with DNA either by intercalation in-between the base pairs or in the minor groove, or both [12]. Therefore, the development of new small molecules capable of binding and nicking of DNA is considered to be a critical aspect in the synthesis of new drugs. The present study is intended to examine the role of molybdenum in form of complex as DNA-nuclease. Although the oxo-molybdenum complexes are found to be good DNA-binders [13], only a very few peroxo-molybdenum-based compounds have been found to exhibit nuclease activity [14]. Hence, the present work has been directed toward the development of artificial DNA nucleases containing oxo-peroxo molybdenum environment. Two oxo diperoxo molybdenum complexes, one with the phenyl acetic acid and other with phenyl hydroxamic acid, have been synthesized. The ligands were chosen so that they have planar moiety along with the oxygen and nitrogen atoms that can establish hydrogen bonds with the DNA which will facilitate DNA cleavage through DNA binding.

## 2. Experimental

### 2.1. Materials and physical methods

Molybdc acid ( $\text{MoO}_3 \cdot 2\text{H}_2\text{O}$ ) and phenyl acetic acid were obtained from S.D. Fine Chemical (India). Hydroxylamine hydrochloride was of extra pure variety and was obtained from Merck (India). Potassium hydroxide pellets and methanol (G.R.) were products of Merck (India) and were used directly. All other reagents used were of G.R. grade and were obtained from Merck (India). Analytical grade solvents used for physicochemical studies were further purified by literature method before use, wherever necessary. Calf-thymus DNA (CT DNA) is a natural DNA widely used in studies of DNA-binding anticancer agents while supercoiled (SC) DNA refers to the over or under winding of a DNA strand (plasmid) marketed as pUC19 DNA, obtained from Sigma Chemical Company, USA, and Genei Bangalore, India, respectively. All DNA solutions were prepared in Tris-HCl buffer at pH 7.4. Other stock solutions were prepared in Tris-HCl buffer. Millipore water was used throughout the course of investigation.

### 2.2. Preparation of the ligand and the molybdenum complexes

#### 2.2.1. Synthesis of *N*-(phenylacetyl)hydroxamic acid (PAHH)

The ligand was prepared by literature method [15]. Methyl phenylacetate was obtained by refluxing the mixture of phenylacetic acid (PAAH) (13.6 g, 0.1 mol) in 25 mL dry methanol followed by addition of 1 mL conc.  $\text{H}_2\text{SO}_4$ . To the above mixture, solid  $\text{NH}_2\text{OH} \cdot \text{HCl}$  (14 g, 0.2 mol) was added followed by the addition of a 25% methanolic KOH (0.4 mol) solution with constant stirring. The reaction mixture was neutralized with 1 N HCl solution, filtered off and the residue was washed with methanol. After evaporation of this methanolic solution a white solid crystalline phenylacetyl hydroxamic acid was obtained. IR (KBr disk,  $\text{cm}^{-1}$ ): 1634(s)  $\nu(\text{C}=\text{O})$ , 1546(m)  $\nu(\text{C}-\text{N})$ .  $^1\text{H}$  NMR ( $\text{CD}_3\text{OD}$ , 300 MHz)  $\delta$  in ppm: 4.8 (s, 1H,  $-\text{OH}$ ), 3.44 (t, 2H,  $-\text{CH}_2-\text{Ar}$ ), 7.226–7.312 (m, 5H, H-benzene ring), 5.46 (s, 1H, NH).

#### 2.2.2. Synthesis of $(\text{PPh}_4)[\text{MoO}(\text{O}_2)_2(\text{PAA})]$ (1)

$\text{MoO}_3$  (0.144 g, 1 mmol) was dissolved in 3 mL  $\text{H}_2\text{O}_2$  (30%, w/v) by stirring at room temperature to get pale yellow solution. Addition of 10 mL methanolic solution of phenylacetic acid (0.136 g, 1 mmol) to the above solution on stirring for 1 h produced a yellow solution. This solution on treatment with  $\text{PPh}_4\text{Br}$  (0.375 g, 1 mmol) dissolved in 10 mL of methanol yielded an orange-yellow solid, which was filtered off. The solid obtained was then washed with water under suction and finally with diethylether, and dried *in vacuo*. Yield: 90%. The crude compound is soluble in acetonitrile, dichloromethane, chloroform, methanol, and ethanol, but insoluble in water, diethyl ether, benzene, and toluene. The compound was crystallized from slow evaporation of methanolic solution to get **1** as yellow crystals. ES  $m/z$  312.92, Anal. Calc for  $\text{C}_{32}\text{H}_{27}\text{O}_7\text{NPMo}$ : C, 57.84; H, 4.10; N, 2.11; Mo, 14.44; P, 4.66. Found: C, 57.14; H, 4.04; N, 2.10; Mo, 14.69; P, 4.73%. IR (KBr,  $\text{cm}^{-1}$ ): 1622(s), 1587(m), 1443(s), 1117(s), 1000(m), 955 (s), 915(s), 855(s), 754(m), 725(s), 692(m), and 526(s). UV-vis ( $\lambda_{\text{max}}$ /nm): 274, 267 and 220.  $^1\text{H}$  NMR ( $\text{CD}_3\text{OD}$ , 300 MHz)  $\delta$  in ppm: 3.5 ( $-\text{CH}_2-\text{Ar}$ ), 6.58–7.74 (m, 5H, H-benzene ring).

### 2.2.3. Synthesis of $(PPh_4)[MoO(O_2)_2(PAH)]$ (**2**)

MoO<sub>3</sub> (0.145 g, ~1 mmol) was dissolved in 3 mL H<sub>2</sub>O<sub>2</sub> (30%, w/v) by stirring at room temperature to get pale yellow solution. Addition of 10 mL methanolic solution of phenyl acetyl hydroxamic acid (0.151 g, 1 mmol) to the above solution on stirring for 1 h produced a yellow solution. This solution on treatment with PPh<sub>4</sub>Br (0.375 g, 1 mmol) dissolved in 10 mL of methanol yielded an orange-yellow solid, which was filtered off. The solid obtained was then washed with water under suction and finally with diethyl ether, and dried *in vacuo*. Yield: 90%. The crude compound is soluble in acetonitrile, dichloromethane, chloroform, methanol and ethanol, but insoluble in water, diethylether, benzene, and toluene. The compound was crystallized by slow evaporation of methanolic solution to get **2** as yellow crystals. ES *m/z* (–) 327.94. Anal. Calc for C<sub>32</sub>H<sub>28</sub>O<sub>7</sub>NPMo: C, 57.75; H, 4.24; N, 2.10; Mo, 14.42; P, 4.65. Found: C, 57.24; H, 4.06; N, 2.06; Mo, 14.29; P, 4.53%. IR (KBr, cm<sup>-1</sup>): 1607(m), 1454(s), 1119(s), 998(m), 959(s), 920(s), 860(s), 767(m), 734(s), 697(m), and 531(s). UV-vis (λ<sub>max</sub>/nm): 276, 268 and 224. <sup>1</sup>H NMR (CD<sub>3</sub>OD, 300 MHz) δ in ppm: 3.4 (–CH<sub>2</sub>–Ar), 7.21–7.84 (m, 5H, H-benzene ring).

### 2.3. X-ray crystal structure determination

X-ray diffraction data for the crystal of **1** was collected at 273 K on a Bruker AXS SMART APEX II diffractometer equipped with a CCD detector [16] with a fine focus of 1.75 kW sealed tube using Mo Kα radiation (λ = 0.71073 Å). Crystallographic data and details of structure determination are summarized in Table 1. The data were processed using SAINT, and absorption corrections were made using SADABS [17]. The structure was solved by direct methods and refined by full-matrix least-squares on the basis of *F*<sup>2</sup> using the WINGX software, using the

**Table 1.** Crystal data and structure refinement parameters of **1**.

Parameters	
Empirical formula	C <sub>32</sub> H <sub>27</sub> O <sub>7</sub> PMo
<i>M</i> <sub>r</sub>	650.45
<i>T</i> /K	273(2)
λ/Å	0.71073
Crystal system	Monoclinic
Space group	P2 <sub>1</sub> /c
<i>Unit cell dimensions</i>	
<i>a</i> /Å	10.0952(3)
<i>b</i> /Å	22.4384(6)
<i>c</i> /Å	12.7546(3)
α/°	90.00
β/°	93.980(2)
γ/°	90.00
<i>V</i> /Å <sup>3</sup>	2882.21(13)
<i>Z</i> , <i>D</i> <sub>c</sub> /g cm <sup>-3</sup>	4, 1.499
<i>F</i> (000)	1328
Crystal size/mm	0.05 × 0.09 × 0.15
θ Range for data collection (°)	1.8, 24.8
Reflections	2,1450
Independent reflections	( <i>R</i> <sub>int</sub> ) 4954(0.035)
Completeness to θ = θ <sub>max</sub> (%)	99.3
Refinement method	Full-matrix least-squares on <i>F</i> <sup>2</sup>
Data/restraints/parameters	4954/0/371
Goodness-of-fit on <i>F</i> <sup>2</sup>	1.027
<i>R</i> indices (all data) [ <i>I</i> > 2σ( <i>I</i> )]	<i>R</i> <sub>1</sub> =0.0315, <i>wR</i> <sub>2</sub> =0.0680, <i>R</i> <sub>1</sub> =0.0438, <i>wR</i> <sub>2</sub> =0.0733
Largest diff. peak, hole/Å <sup>-3</sup>	–0.331, 0.274

SHELX suites [18]. The non hydrogen atoms were refined anisotropically, while the hydrogens were placed with fixed thermal parameters at idealized positions. Perspective views of the molecules were obtained by Mercury [18].

## 2.4. Computational studies of 2

The DFT calculations were carried out using the Gaussian09 program [19] using the hybrid density functional theory (B3LYP) method. The 6-311G\* basis set was used to describe C, N, O, P, and 6-31G\* basis set for hydrogen atoms [20]. The Mo atom was described using the LANL2DZ basis set [21]. The full geometry optimizations were carried out for **2**. To compute the UV-vis transitions of **2**, the singlet-excited state geometries corresponding to the vertical excitations were optimized using the time-dependent DFT (TD-DFT) scheme starting with the ground state geometries. The percentages of the contributions for the vertical excitations were calculated using Gauss sum 2.1.

## 2.5. DNA binding studies

### 2.5.1. UV-vis spectral study

The solutions of CT DNA in Tris-HCl/NaCl buffer medium (50 mM Tris-HCl and 50 mM NaCl, pH 7.2) gave a ratio of  $A_{260}/A_{280}$  of ca. 1.8–1.85, indicating that the DNA was sufficiently free from protein contamination [22]. The DNA concentration per nucleotide was determined by absorption spectroscopy using the molar absorption coefficient  $6600 \text{ M}^{-1} \text{ cm}^{-1}$  at 260 nm [22]. Stock solutions were stored at 4 °C and used within four days.

UV-vis spectra were recorded in a Shimadzu UV-1700 spectrophotometer. The electronic spectra of **1** and **2** were monitored in the presence and absence of DNA. In this absorption titration experiment, a fixed concentration of **1** or **2** was titrated with increasing amounts of DNA over a range of 0–200  $\mu\text{M}$  in appropriate cases. To eliminate the absorbance of DNA, equal amounts of DNA were added to the reference solution as well. The intrinsic binding constant was determined by using eqn. (1) [23]:

$$[\text{DNA}]/(\epsilon_a - \epsilon_f) = [\text{DNA}]/(\epsilon_b - \epsilon_f) + 1/[K_b(\epsilon_b - \epsilon_f)] \quad (1)$$

Here, [DNA] is the concentration of DNA in base pairs, the apparent absorption coefficients  $\epsilon_a$ ,  $\epsilon_f$  and  $\epsilon_b$  corresponds to  $A_{\text{obsd}}/[\text{complex}]$ , the extinction coefficient for the free complex, and the extinction coefficient for the complex in the fully bound form, respectively. Plots of  $[\text{DNA}]/(\epsilon_a - \epsilon_f)$  versus [DNA] gave a slope  $1/(\epsilon_b - \epsilon_f)$  with Y-intercept  $1/[K_b(\epsilon_b - \epsilon_f)]$ . The intrinsic binding constant  $K_b$  was obtained from the ratio of the slope to the intercept.

### 2.5.2. Viscometric study

Viscosity of sonicated DNA [24] (average molecular weight of ~200 base pairs was made by using a Labsonic 2000 sonicator) was measured by a fabricated micro viscometer, maintained at 28 ( $\pm 0.5$ ) °C in thermostatic water bath. The viscosities of CT DNA, CT DNA-ligand, CT DNA-**1**, and CT DNA-**2** were measured. Data were presented as  $(\eta/\eta_0)^{1/3}$  versus the ratio of the concentration of the ligand or complexes **1** or **2** to that of the CT DNA, where  $\eta_0$  is the viscosity of CT DNA solution alone and  $\eta$  is the viscosities of CT DNA solution in the presence of the complexes or the ligand. Viscosity values were calculated from the observed flow time

of CT DNA by the relation  $\eta = t - t_0$ , where  $t$  and  $t_0$  are the values of flow times for the solution and the buffer, respectively.

### 2.5.3. Cyclic voltammetry study

Electrochemical measurements were performed using a PAR Versa Stat-potentiostat/Galvanostat II electrochemical analysis system by purging with purified nitrogen. The reference electrode used was saturated Ag/AgCl/KCl, which was isolated from the solution by salt bridge to prevent contamination through leakage from the electrode. The auxiliary and working electrodes were platinum foil and carbon paste electrode that were placed directly to the solution. The cyclic voltammetric (CV) measurement was carried out at 25 °C in buffer solution, and the concentration of the supporting electrolyte KCl was maintained at 0.1 M. All potentials reported in this study were referenced against the Ag/AgCl electrode. Pure CT DNA and blank solution are electrochemically inactive in the potential range of + 1.5 V to -1.25 V under our experimental conditions.

### 2.5.4. Gel electrophoresis study

The DNA cleavage activity of the complexes was monitored using agarose gel electrophoresis. The super coiled (SC) pUC19 DNA (0.5  $\mu\text{g}$  per reaction) in Tris-HCl buffer (50 mM) with 50 mM of NaCl (pH 7.2) was treated with  $\text{H}_2\text{O}_2$ , and the appropriate amount of the complex followed by dilution with the Tris-HCl buffer to a total volume of 15  $\mu\text{L}$  and then incubated for 1 h at 37 °C. After incubation it was mixed with a loading buffer containing 25% bromophenol blue, 30% glycerol (3  $\mu\text{L}$ ) and was loaded on a 0.9% agarose gel containing 1.0  $\mu\text{g mL}^{-1}$  ethidium bromide (EB). Electrophoresis was carried out at 60 V for 3 h in TAE buffer (40 mM Tris, 20 mM acetic acid, 1 mM EDTA, pH 7.2). The bands were visualized by UV light and photographed. The cleavage of SC pUC19 DNA induced by the complex was photographed with the UVP BIO-DOC-IT Gel Documentation System, and the extent of nicking induced by the complexes was determined by analyzing the intensities of the bands using UVP – BIO-DOC-IT LS Software.

## 2.6. Molecular docking

The rigid molecular docking studies were performed by using HEX 6.3 [25] software (<http://www.loria.fr/~ritchied/hex/>). For the Docking study, the coordinates of **1** were taken from its crystal structure as a CIF file and converted to the PDB format using Mercury software (<http://www.ccdc.cam.ac.uk/>) and for **2** coordinates were taken from the DFT optimized structure and converted to the PDB format, and the geometries of **1** and **2** were optimized by applying CHARMM force field in Discovery studio 3.1. The crystal structure of the B-DNA dodecamer d(CGCGAATTCGCG)<sub>2</sub> (PDB ID: 1BNA) was downloaded from the protein data bank (<http://www.rcsb.org/pdb>). All calculations were carried out on an Intel I5, 3.1 GHz based machine with MS Windows 7 as the operating system. Visualization of the docked pose has been done by using Discovery studio 3.1 and PyMol (<http://pymol.sourceforge.net/>) molecular graphics program.

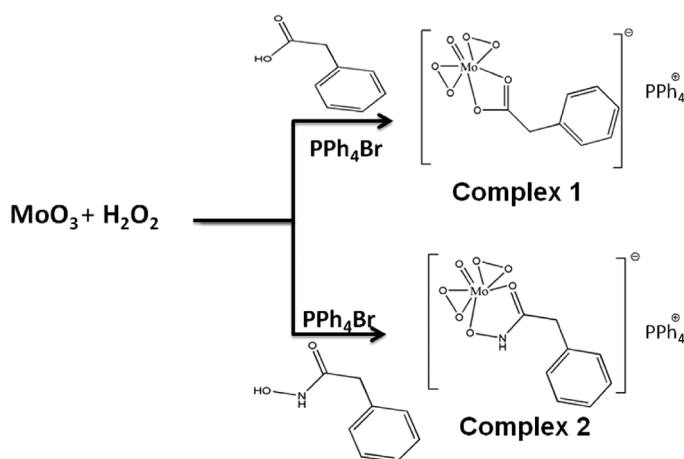
### 3. Results and discussion

#### 3.1. Synthetic aspects of the complexes

Complexes **1** and **2** were synthesized by following Scheme 1. The complexes are stable in air. Diffractable yellow single-crystal of **1** was obtained by slow evaporation of a methanolic solution.

#### 3.2. Spectral characterization of the complexes

The IR spectra show strong  $\nu(\text{Mo}=\text{O})$  vibration at 955 and 959  $\text{cm}^{-1}$  in **1** and **2**, respectively. The corresponding  $\nu(\text{O}-\text{O})$  vibration appears as medium intensity bands at 855 and 915  $\text{cm}^{-1}$  in **1** and at 860 and 920  $\text{cm}^{-1}$  in **2**. In free PAAH, the  $\nu(\text{C}=\text{O})$  vibration occurs at 1622  $\text{cm}^{-1}$  which on coordination with Mo(VI) shifts to 1587  $\text{cm}^{-1}$  in **1**, whereas the  $\nu(\text{C}=\text{O})$  of free PAHH at 1634  $\text{cm}^{-1}$  is shifted to 1607  $\text{cm}^{-1}$  after coordination in **2**. The shifting of  $\nu(\text{C}=\text{O})$  to lower energy region indicates the decrease in C = O bond order due to drainage of electron density from carbonyl oxygen to Mo-center. The vibrations at 646  $\text{cm}^{-1}$  and 584  $\text{cm}^{-1}$  in **1** and at 642  $\text{cm}^{-1}$  and 578  $\text{cm}^{-1}$  in **2** appear as weak bands which are assignable to asymmetric and symmetric vibrations, respectively, of the  $\text{MO}_2$  triangle formed by the engagement of the terminal  $\text{O}_2^{2-}$  ligand. The bands at 1443, 1117, 995, 754, 725, 692, and 526  $\text{cm}^{-1}$  in **1** and 1454, 1119, 998, 767, 734, 697, and 531  $\text{cm}^{-1}$  in **2** appear due to the  $\text{Ph}_4\text{P}^+$  moiety. Molar conductivity values in acetonitrile solution of **1** and **2** are 148  $\text{ohm}^{-1}\text{cm}^2\text{mol}^{-1}$  and 134  $\text{ohm}^{-1}\text{cm}^2\text{mol}^{-1}$ , respectively. This indicates that both complexes are 1:1 electrolytes [26]. The electronic spectra of the free phenyl acetic acid and phenyl acetyl hydroxamic acid ligands show a broad peak at 230 nm and 249 nm, respectively, which correspond to intra-ligand  $\pi \rightarrow \pi^*$  transitions of the aromatic ring. The bands are shifted to 222 nm for **1** and 226 nm for **2**, respectively. Two bands appear at 267 nm, 274 nm for **1** and 268 nm, 276 nm for **2** due to the  $n \rightarrow \pi^*$  of C=O functional group of both coordinated ligands. This low energy shift is due to the drainage of electron density of  $-\text{C}=\text{O}-$  bond through the coordination of O atom to the metal center in the complexes [13].



**Scheme 1.** Synthetic scheme of **1** and **2**.

The  $^1\text{H}$  NMR spectroscopic study confirmed that **1** and **2** as well as the ligands are stable in solution phase. In **2** the hydroxamate  $-\text{OH}$  is deprotonated, which is characterized by the disappearance of the  $-\text{OH}$  proton signal at  $\delta$  4.8 ppm, whereas in **1**,  $-\text{COOH}$  proton of phenylacetate ligand is deprotonated which is evidenced by the non-appearance of the  $-\text{COOH}$  proton signal at  $\delta$  9.8 ppm. This suggests that both ligands behave as mono-anionic O,O-donor centers. The methylene proton signal ( $-\text{CH}_2$ ) is observed around  $\delta$  3.5 ppm for **1** and at  $\delta$  3.4 ppm for **2**. The aromatic proton signals at 6.58–7.74 ppm and 7.21–7.84 ppm are owed to intermixing of the signals of the aromatic protons of phenyl group of the phenyl moiety and those for the  $\text{PPh}_4$  groups in both **1** and **2**, respectively, and have appeared as multiplets.

### 3.3. Structural characterization of the complexes

#### 3.3.1. Crystal structure of **1**

Crystal structure of **1** consists of discrete monomeric anions  $[\text{MoO}(\text{O}_2)_2(\text{PAA})]^-$  and tetraphenylphosphonium  $[\text{PPh}_4]^+$  cations (see Figure 1 for the ORTEP view). The crystallographic parameters of **1** are shown in Table 1. Complex **1** crystallizes in the monoclinic  $\text{P}2_1/n$  space group with the unit cell dimensions of  $a = 10.0952 \text{ \AA}$ ,  $b = 22.4384 \text{ \AA}$ ,  $c = 12.7546 \text{ \AA}$ ,  $\alpha = 90.0^\circ$ ,  $\beta = 93.98^\circ$ ,  $\gamma = 90.0^\circ$ . The coordination geometry around the metal atom is found to be pentagonal bipyramidal with the axial sites being occupied by the carbonyl oxygen (O1) and the oxo (O7) ligands. The carboxylate oxygen (O2) and the peroxy moieties (O3, O4 and O5, O6) define the equatorial plane whereas the Mo atom is displaced by  $[-0.324(1) \text{ \AA}]$  from the equatorial plane towards the oxo-oxygen (O7). This is consistent with the observations in oxodiperoxo molybdenum(VI) complexes which generally feature the metal atom coordination to the oxo-group in the axial position and the two peroxy groups bound in the equatorial positions. The chelated phenylacetyl moiety (C1–C7, O2, O1) is essentially planar and is approximately orthogonal to the equatorial plane (O2,O3–O6); the dihedral angle between the two planes is  $78.3(1)^\circ$ . Selected bond distances and angles for **1** (Table 2) correspond to those of other seven-coordinate Mo-oxoperoxo complexes [27]. The lengthening

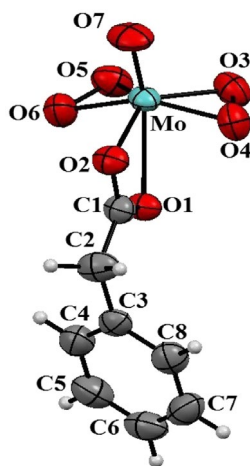


**Figure 1.** ORTEP representation of the X-ray crystal structure of anionic part of **1** with all non-hydrogen atoms shown as 50% thermal ellipsoids.

**Table 2.** Selected bond lengths (Å) and angles (°) of **1**.

Bond lengths (Å)			
Mo–O1	2.428(17)	Mo–O6	1.936(2)
Mo–O2	2.084(18)	Mo–O7	1.662(19)
Mo–O3	1.909(19)	O3–O4	1.462(3)
Mo–O4	1.948(2)	O5–O6	1.469(3)
Mo–O5	1.913(2)		
Bond angles (°)			
O2–Mo1–O1	57.06(6)	O7–Mo1–O4	102.20(10)
O4–Mo1–O1	78.02(8)	O5–Mo1–O6	44.87(9)
O6–Mo1–O1	77.95(8)	O3–Mo1–O6	129.58(9)
O5–Mo1–O1	93.35(8)	O7–Mo1–O6	102.90(11)
O3–Mo1–O1	93.30(8)	O3–Mo1–O5	87.23(9)
O7–Mo1–O1	153.84(9)	O7–Mo1–O5	105.69(11)
O4–Mo1–O2	85.79(8)	O7–Mo1–O3	105.17(10)
O6–Mo1–O2	87.88(8)	O3–Mo1–O4	44.53(9)
O5–Mo1–O2	130.69(8)	O5–Mo1–O4	129.29(9)
O3–Mo1–O2	128.47(9)	O6–Mo1–O4	154.66(9)
O7–Mo1–O2	96.78(9)		

**Table 3.** Relevant intermolecular hydrogen bonds (Å) in **1**.

D–H...A	d(D–H)	d(H...A)	d(D...A)	∠(DHA) <sup>o</sup>
C24–H23...O1 <sup>a</sup>	0.93	2.54	3.438(4)	161
C24–H24...O1 <sup>a</sup>	0.93	2.47	3.145(3)	130
C19–H19...O5 <sup>b</sup>	0.93	2.55	3.161(4)	124

<sup>a</sup>1/2 + x, 3/2 – y.<sup>b</sup>–1/2 + z, 1 – x, 2 – y, 2 – z.

of the Mo–O1 [2.428(17) Å] distances in **1** compared to the Mo–O [2.194(3)–2.269(3) Å] bond lengths in complexes where the ligand oxygen atoms coordinate the metal center equatorially reflects the strong *trans* influence of the oxo-ligand [27]. In addition to the strong intramolecular O–H...O hydrogen bond [O6...O3, 2.764(2) Å in case of **1**], some weak intermolecular C–H...O hydrogen bonds between the anions (Table 3) are also present, and these interactions stabilize the structure in **1** (Figure 2).

### 3.3.2. Structures of **1** and **2**: density functional theory calculations

Geometry optimization for **1** and **2** has been carried out at the DFT level. The Mo atom was described using the LANL2DZ basis set while the 6-311G\* basis set was used to describe C, N, O, P and 6-31G\* basis set for hydrogen atoms [20] (Figure 3). The initial geometries were taken from the single-crystal X-ray data of **1** and subjected to optimization. The geometrical parameters *viz.* bond lengths and bond angles were calculated (Table 4) using the Gaussian 09 package [19]. Contour plots of molecular orbitals of the complexes were generated using Gauss view 5.0 and the frontier molecular orbitals in **1** and **2** were calculated (Figure 3). The DFT calculation confirms the optimized structure of **2**. It is seen that the highest occupied molecular orbital (HOMO) is localized largely on the Mo atom and peroxo oxygen in **1** and **2**. However, the lowest unoccupied molecular orbital (LUMO) is localized largely on the phenyl ring of both ligands. The calculated HOMO energies of the complexes vary as **1** (–5.32 eV) < **2** (–5.91 eV) and those of LUMO exhibit a similar trend: **1** (–3.27 eV) < **2** (–3.68 eV). Upon introducing a hydroxamic group in **1** to obtain **2**, both HOMO and LUMO energies increase, and interestingly, the increase in HOMO energy is more pronounced than

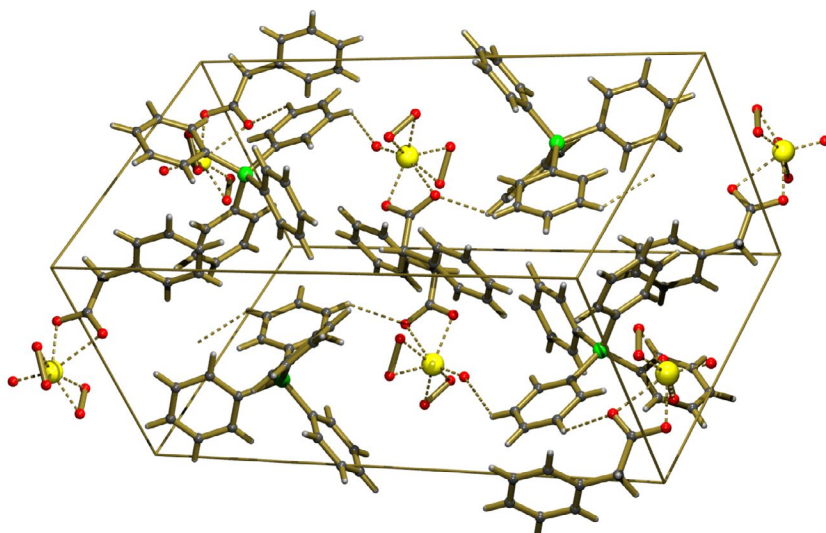


**Figure 2.** Packing pattern showing H-bonding in **1**.

that in LUMO energy. It is noteworthy that upon incorporating hydroxamic groups into the phenylacetato ligand in **1** to obtain **2**, the changes in both HOMO and LUMO energies are not significant revealing that the coordination of the ligand does not affect the HOMO and LUMO energy levels. This clearly supports that the HOMO orbitals in **1** and **2** are localized on the peroxy moiety. The HOMO–LUMO energy gaps in **1** (2.45 eV) and **2** (2.23 eV) are almost the same, which is consistent with other reported Mo-complexes [21].

The UV–vis spectrum of **2** in acetonitrile solution has also been explored by using a TD-DFT approach. The calculated absorption energies, their associated oscillator strengths, the main configurations and their assignments are given in Table 5, while the combined experimental and simulated UV–vis spectra of **2** are displayed in Figure 4(A). The experimental wavelengths do not exactly match with the theoretical one, but all the transitions are found in the theoretically generated spectra with very nominal shifts.

The structure of oxo-diperoxo complex **2** was further supported by IR frequency calculations which were obtained by DFT. The  $\nu(\text{O}-\text{O})$  vibrations at  $946$  and  $871\text{ cm}^{-1}$  and  $\nu(\text{Mo}=\text{O})$  vibrations at  $1102\text{ cm}^{-1}$  and for  $\nu(-\text{C}=\text{O})$  frequency at  $1596\text{ cm}^{-1}$  (Figure 4(B)) obtained from the above calculations are within the tolerance limit with the value obtained experimentally (Table 6).

### 3.4. DNA binding studies

The present study is directed toward the development of synthetic DNA nucleases, so, establishment of the ability to damage the double stranded DNA by a given molecule demands a thorough study on the interaction of DNA with the potential nuclease molecule. Hence, the binding of DNA by the synthetic molecules has been studied, results of which are being presented herein.

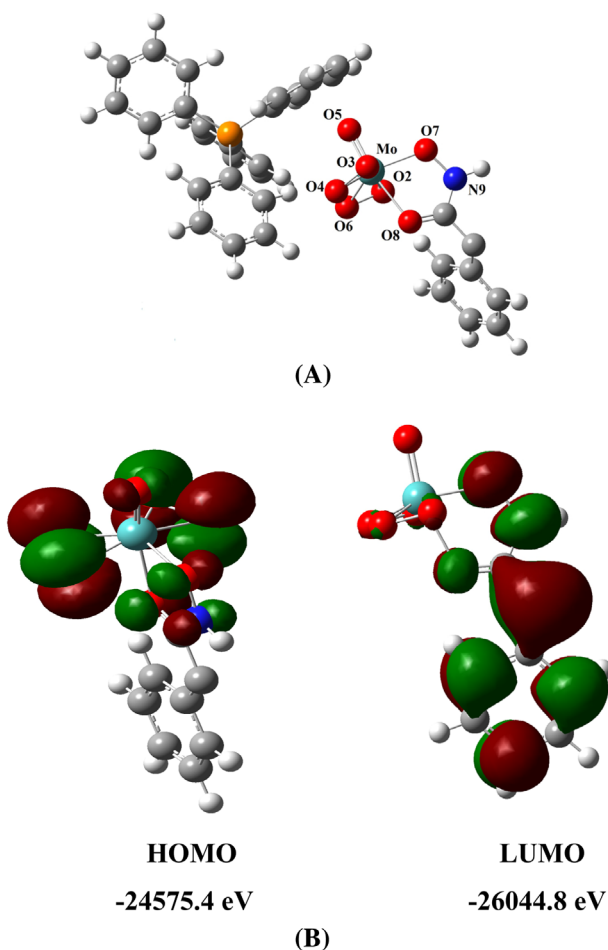


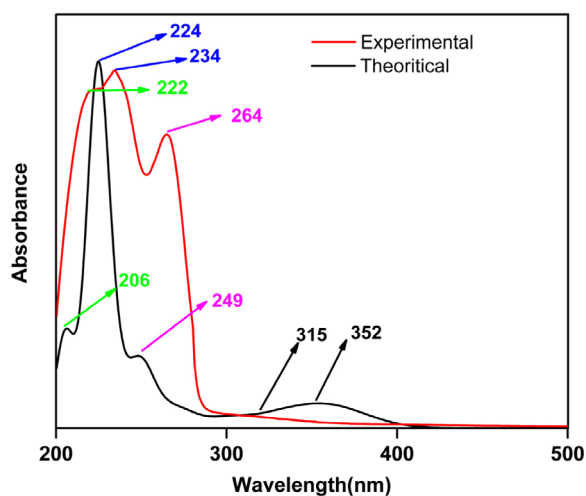
**Figure 3.** (A) LANL2DZ and 6–31G\* ground state optimized geometry of **2**; (B) showing HOMO and LUMO of anionic part of **2**.

**Table 4.** Theoretically calculated selected interatomic distances (Å) and bond angles (°) for **2**.

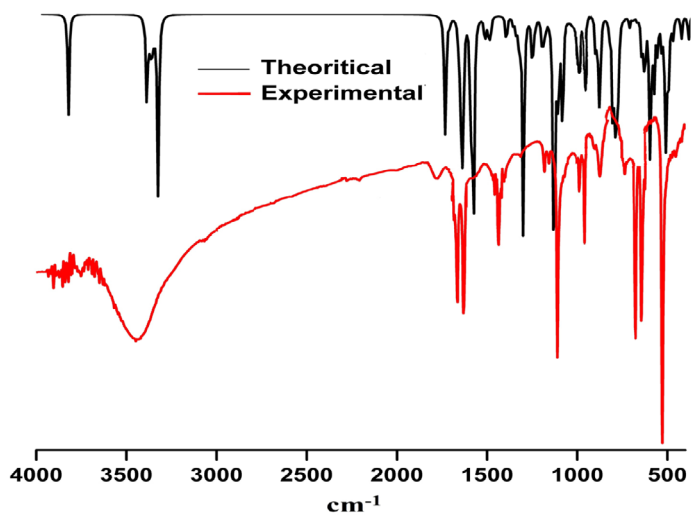
Bond lengths (Å)			
Mo–O5	1.72205	Mo–O5	1.97588
Mo–O3	2.01051	Mo–O7	2.18373
Mo–O4	1.97534	Mo–O8	2.34743
Mo–O2	2.00969	N9–O7	1.35992
N9–H23	1.01781		
Bond angles (°)			
O5–Mo–O2	101.52442	O3–Mo–O2	156.68130
O5–Mo–O6	104.76133	O3–Mo–O5	130.59589
O5–Mo–O3	101.51411	O2–Mo–O4	130.58212
O5–Mo–O4	104.79151	O4–Mo–O7	132.05222
O5–Mo–O7	90.50030	O3–Mo–O7	88.11875
O5–Mo–O8	162.14968	O2–Mo–O7	88.12613
O7–Mo–O6	132.07420		

**Table 5.** Selected UV–vis energy transitions at the TD-DFT/B3LYP level for **2** in acetonitrile.

$\lambda_{\text{cal}}$ (nm)	Oscillator strength ( $f$ )	$\lambda_{\text{expt}}$ (nm)	Key transitions
352	0.0089	315	H-3->LUMO (64%), H-2->L+1 (14%), HOMO->LUMO (11%), H-2->L+2 (5%), H-1->LUMO (2%)
249	0.0161	264	H-7->LUMO (31%), H-6->LUMO (52%) H-11->L+1 (4%), H-5->L+1 (5%), HOMO->L+3 (3%)
224	0.1444	232	H-7->LUMO (11%), H-7->L+1 (16%), H-5->L+2 (33%) H-11->LUMO (5%), H-6->LUMO (6%), H-6->L+3 (5%), H-5->L+3 (6%), H-4->L+3 (2%)
206	0.056	222	H-1->L+7 (15%), H-1->L+8 (17%), HOMO->L+7 (28%), HOMO->L+8 (27%), H-6->L+3 (5%)



(A)



(B)

**Figure 4.** (A) Calculated (black) and experimental (red) absorption spectra of **2** in acetonitrile at room temperature. (B) Calculated (black) and experimental (red) infrared spectra of **2**.

**Table 6.** Comparisons of experimental and theoretical stretching frequency (in  $\text{cm}^{-1}$ ) of **2**.

Frequency	Theoretical values	Experimental values	% of deviation
$\nu(\text{C}=\text{O})$	1596	1607	0.7
$\nu(\text{N}-\text{H})$	1415	1454	2.7
$\nu(\text{Mo}=\text{O})$	1102	959	13
$\nu(\text{O}-\text{O})$	946,871	920,860	3.0, 1.3
$\nu[\text{MO}_2(\text{triangle})]$	662,529	642,578	3.0, 8.0

### 3.4.1. Electronic absorption spectral studies

Electronic absorption spectroscopy is utilized to examine the binding of metal complexes with DNA. The electronic spectra of both **1** and **2** (Figures 5 and 6) were monitored in the presence and absence of DNA. Upon addition of incremental amounts of DNA, the intensity of the bands at 267 and 274 nm for **1** and 268 and 276 nm for **2** increased. This increase in the absorptivity and red shift (4 nm) of both **1** and **2** support that the interaction occurred of both complexes in the groove of CT DNA [13, 28]. Hoechst 33258 family groove binders also exhibit red shifts of absorption bands when they bind to the grooves of a DNA helix [29]. A plot of  $[\text{DNA}]/(\epsilon_a - \epsilon_f)$  versus  $[\text{DNA}]$  gives the binding constants which were calculated to be  $(5.2 \pm 0.2) \times 10^4 \text{ M}^{-1}$  for DNA-complex **1** and  $(7.3 \pm 0.2) \times 10^4 \text{ M}^{-1}$  for DNA-complex **2**. Complexes **1** and **2** show identical DNA-binding affinities as both of them have identical ligand environment with phenyl aromatic ring involved. Due to the absence of planarity of the complexes, they compromise the weaker electrostatic interaction imparted by the negatively charged phosphate groups of DNA.

### 3.4.2. Viscometric studies

The measurement of DNA-viscosity is a sensitive technique to understand the mode of DNA-binding [30]. The relative viscosity of CT DNA solution is known to increase on intercalative binding of substrates, because the insertion of intercalators causes the base pairs of the DNA to get apart and thus causes lengthening of the DNA helix, while molecules bound to DNA through groove do not alter the relative viscosity of DNA, and the partial or non-classical intercalation of ligand may bend or kink the DNA helix, thereby decreasing its effective length and subsequently viscosity [30]. The values of relative specific viscosities of DNA in the absence and presence of **1** and **2** are plotted against  $[\text{complex}]/[\text{DNA}]$  (Figure 7). It is observed that the addition of either **1** or **2** to the CT DNA solution does not show significant increase in the viscosity of CT DNA, thereby clearly demonstrating the groove-binding of CT DNA by the present complexes **1** and **2**.

### 3.4.3. Electrochemical investigation of **1** and **2** with DNA

Electrochemical investigation of the metal complex-DNA interaction provides a useful complement to the spectroscopic methods. It is known that the electrochemical potential of metal complexes will shift positively when it intercalates into DNA, and if it is bound to DNA by electrostatic interaction, the potential would shift in a negative direction [31]. Cyclic voltammograms (CV) of **1** and **2** in the absence and presence of CT DNA in Tris-HCl buffer solution are shown in Figures 8 and 9.

The quasi-reversible redox couples for **1** and **2** in acetonitrile:buffer (1:9) solution have been studied upon addition of CT DNA and the shifts of the cathodic ( $E_{pc}$ ) and anodic ( $E_{pa}$ ) potentials are recorded. No new redox peaks appeared after the addition of CT DNA to **1**

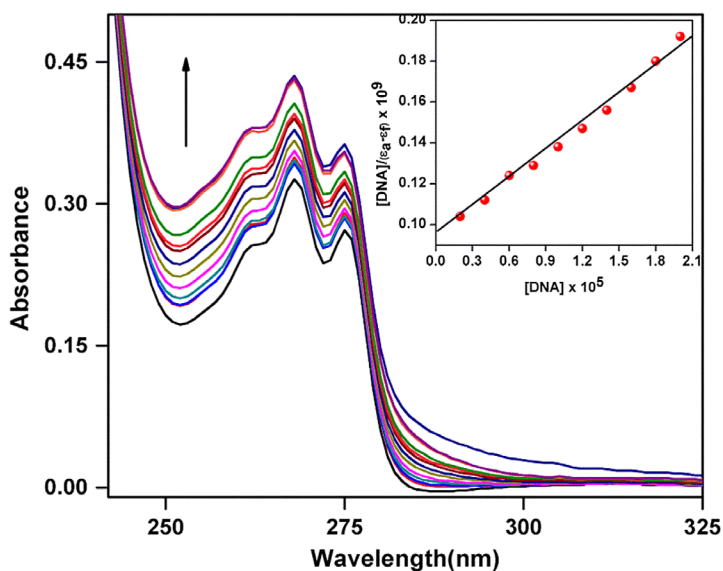


**Figure 5.** Absorption spectra of **1** ( $60 \mu\text{M}$ ) in the presence of increasing amounts of CT DNA,  $[\text{DNA}]/[\text{complex}] = (a - l)$ :  $0-200 \mu\text{M}$ . (Inset: plot of  $\{[\text{DNA}]/(\varepsilon_a - \varepsilon_f)\} \times 10^9 \text{ M/M}^{-1} \text{ cm}^{-1}$  vs.  $[\text{DNA}] \times 10^5 \text{ M}$ ).

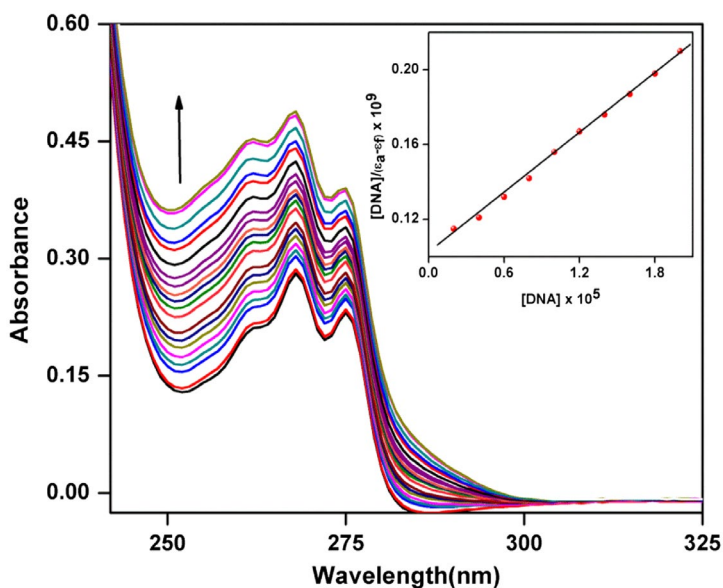


**Figure 6.** Absorption spectra of **2** ( $60 \mu\text{M}$ ) in the presence of increasing amounts of CT DNA,  $[\text{DNA}]/[\text{complex}] = (a - l)$ :  $0-200 \mu\text{M}$ . (Inset: plot of  $\{[\text{DNA}]/(\varepsilon_a - \varepsilon_f)\} \times 10^9 \text{ M/M}^{-1} \text{ cm}^{-1}$  vs.  $[\text{DNA}] \times 10^5 \text{ M}$ ).

and **2**, but the current intensity of all the peaks increased significantly, suggesting the existence of an interaction between **1** and **2** and CT DNA. The increase or decrease in current intensity can be explained in terms of an equilibrium mixture of free and DNA-bound complex to the electrode surface [32]. In both **1** and **2**, with increasing concentration of CT DNA,

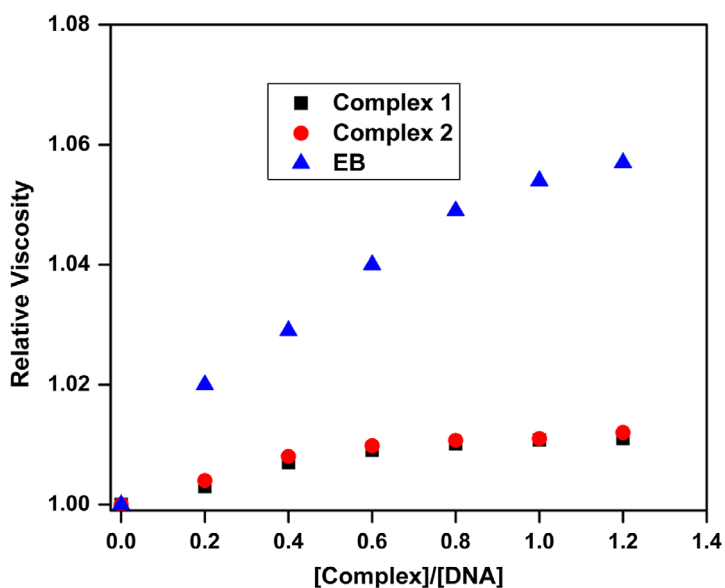


**Figure 7.** Effect of increasing the amount of 1, 2 and EB on the specific viscosity of CT DNA.

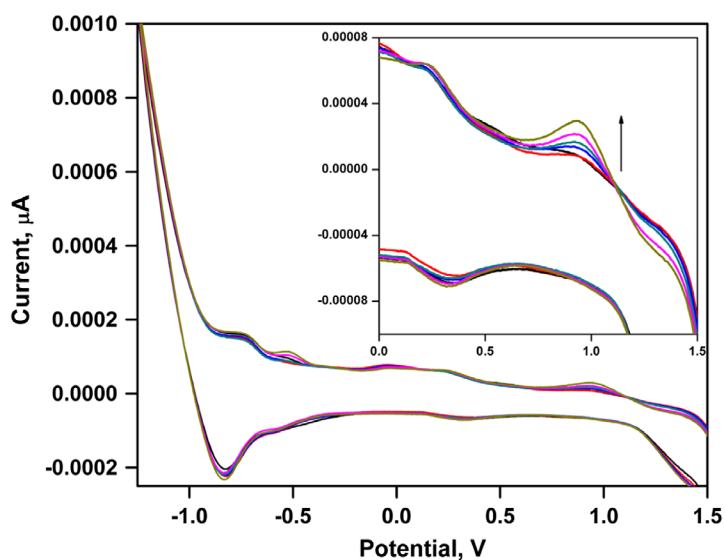


**Figure 8.** Cyclic voltammogram of interaction of 1 and CT DNA. [CT DNA] = 0.0, 50, 100, 150, 200  $\mu\text{M}$ . Scan rate: 80  $\text{mV s}^{-1}$ .

the cathodic peak potentials of the complexes shifted toward lower values, indicating the non-intercalative binding nature of the complexes with CT DNA. For **1** the shift of cathodic peak potential is 0.947 to 0.929 V, whereas the shift observed for **2** is 0.942 to 0.9031 V after addition of CT DNA. This shift in peak potentials supports the non-intercalative binding nature of **1** and **2** with CT DNA.

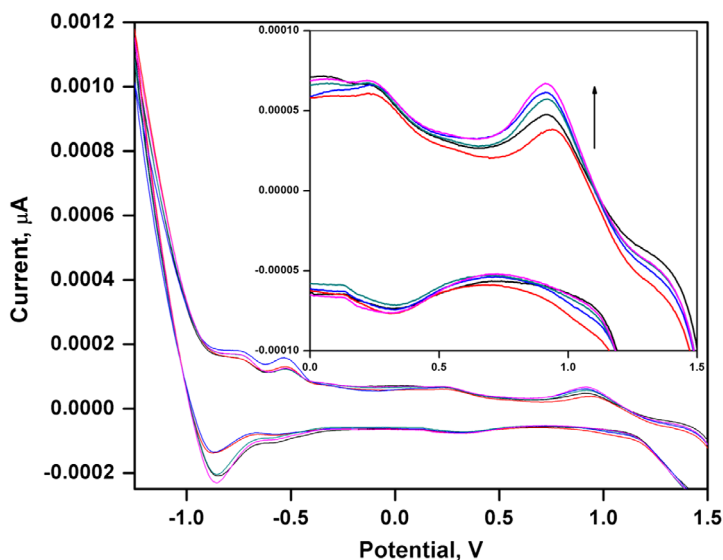


**Figure 9.** Cyclic voltammogram of interaction of **2** and CT DNA. [CT DNA] = 0.0, 50, 100, 150, 200  $\mu\text{M}$ . Scan rate: 80  $\text{mV s}^{-1}$ .

#### 3.4.4. Nuclease activity

The nuclease activity of the complexes has been studied using supercoiled (SC) pUC19 DNA. The naturally occurring supercoiled form (Form I), nicked to circular (NC) plasmid with one DNA-strand is cut by releasing the supercoiling and leaves a large floppy circle, may give rise to linear and open circular relaxed forms, Forms II and III, respectively. Form I migrates relatively faster in comparison to Forms II and III. The electrophoretic pattern of plasmid DNA treated with **1** and **2** are shown in Figure 10. Firstly, the concentration-dependent DNA cleavage experiments by **1** and **2** were monitored.

Complexes **1** and **2** (at concentration of 20  $\mu\text{M}$ ) converted the SC DNA into NC relaxed form of DNA by 20% and 22%, respectively (Figure 10). The result indicated that **1** and **2** have exhibited weak nuclease activity toward SC DNA (pUC19) (Table 7). The present experiment suggests that untreated DNA and DNA incubated with peroxide alone did not show any significant DNA cleavage (lanes 1 and 2 in Figure 10). However, in the presence of peroxide, **1** and **2** were found to exhibit good nuclease activity (Figure 11, Table 8). The presence of  $\text{H}_2\text{O}_2$  as an oxidizing agent leads to the formation of ROS ( $\text{OH}^\cdot$ ) through the Fenton type mechanism, which helps metal complex mediated DNA cleavage [33]. It is observed that **2** is more effective in nicking pUC19 DNA either alone or in combination with  $\text{H}_2\text{O}_2$  than **1**. The control experiments suggest that untreated plasmid DNA (lane 1) contains 90% (SC) and 10% (NC). The treatment of this DNA with incremental amounts (10  $\mu\text{M}$ , 20  $\mu\text{M}$ , and 30  $\mu\text{M}$ ) of either **1** or **2** induces a substantial cleavage of DNA in the presence of  $\text{H}_2\text{O}_2$ . It is interesting to note that both complexes are capable of inducing both NC and linear form under the present experimental setup.

Concentration-dependent DNA cleavage experiments were carried out in the presence of fixed concentration of  $\text{H}_2\text{O}_2$  (30  $\mu\text{M}$ ) by varying the concentration of **1** and **2** (10–30  $\mu\text{M}$ ). At 20  $\mu\text{M}$  concentration of **1** and **2**, significant DNA cleavage (NC DNA) 56% and 72% (Figure

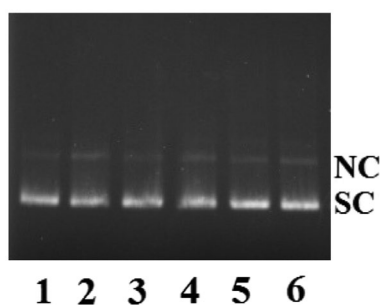


**Figure 10.** Agarose gel (9%) electrophoregram of supercoiled pUC19 DNA (0.5  $\mu\text{g}$ ) incubated for 45 min at 37  $^{\circ}\text{C}$  in a buffer containing 50 mM Tris–HCl and 50 mM NaCl at 37  $^{\circ}\text{C}$  pH 7.2 with increasing concentrations of **1** and **2**. Lane 1: DNA control; Lane 2, DNA +  $\text{H}_2\text{O}_2$  (30  $\mu\text{M}$ ); Lane 3, DNA + **1** (10  $\mu\text{M}$ ); Lane 4, DNA + **1** (20  $\mu\text{M}$ ); Lane 5, DNA + **2** (10  $\mu\text{M}$ ); Lane 6, DNA + **2** (20  $\mu\text{M}$ ).

**Table 7.** pUC19 plasmid DNA cleavage by **1** and **2**.

Lane no.	Reaction condition	Form I (% SC)	Form II (% NC)
1	pUC 19 DNA CONTROL	90	10
2	pUC 19 + 30 $\mu\text{M}$ $\text{H}_2\text{O}_2$	87	13
3	pUC 19 + 10 $\mu\text{M}$ complex <b>1</b>	86	14
4	pUC 19 + 20 $\mu\text{M}$ complex <b>1</b>	80	20
5	pUC 19 + 10 $\mu\text{M}$ complex <b>2</b>	83	17
6	pUC 19 + 20 $\mu\text{M}$ complex <b>2</b>	78	22

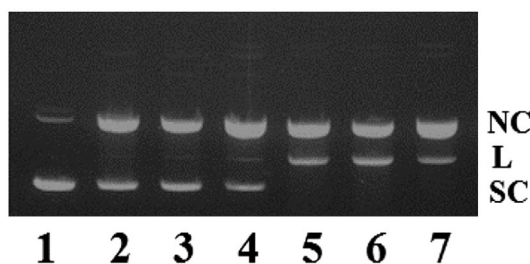


**Figure 11.** Agarose gel (9%) electrophoregram of supercoiled pUC19 DNA (0.5  $\mu\text{g}$ ) incubated for 45 min at 37  $^{\circ}\text{C}$  in a buffer containing 50 mM Tris–HCl and 50 mM NaCl at 37  $^{\circ}\text{C}$  pH 7.2 with increasing concentrations of **1** and **2**. Lane 1: DNA control; Lane 2, DNA +  $\text{H}_2\text{O}_2$  (30  $\mu\text{M}$ ) + **1** (10  $\mu\text{M}$ ); Lane 3, DNA +  $\text{H}_2\text{O}_2$  (30  $\mu\text{M}$ ) + **2** (10  $\mu\text{M}$ ); Lane 4, DNA +  $\text{H}_2\text{O}_2$  (30  $\mu\text{M}$ ) + **1** (20  $\mu\text{M}$ ); Lane 5, DNA +  $\text{H}_2\text{O}_2$  (30  $\mu\text{M}$ ) + **2** (20  $\mu\text{M}$ ); Lane 6, DNA +  $\text{H}_2\text{O}_2$  (30  $\mu\text{M}$ ) + **1** (30  $\mu\text{M}$ ); Lane 7, DNA +  $\text{H}_2\text{O}_2$  (30  $\mu\text{M}$ ) + **2** (30  $\mu\text{M}$ ).

**Table 8.** pUC19 plasmid DNA cleavage by complexes **1** and **2** in presence of  $\text{H}_2\text{O}_2$ .

Lane no.	Reaction condition	Form I (% SC)	Form III (%L)	Form II (% NC)
1	pUC 19 DNA CONTROL	90		10
2	pUC 19 + 30 $\mu\text{M}$ $\text{H}_2\text{O}_2$ + 10 $\mu\text{M}$ complex <b>1</b>	45		55
3	pUC 19 + 30 $\mu\text{M}$ $\text{H}_2\text{O}_2$ + 10 $\mu\text{M}$ complex <b>2</b>	47		53
4	pUC 19 + 30 $\mu\text{M}$ $\text{H}_2\text{O}_2$ + 20 $\mu\text{M}$ complex <b>1</b>	40	4	56
5	pUC 19 + 30 $\mu\text{M}$ $\text{H}_2\text{O}_2$ + 20 $\mu\text{M}$ complex <b>2</b>		28	72
6	pUC 19 + 30 $\mu\text{M}$ $\text{H}_2\text{O}_2$ + 30 $\mu\text{M}$ complex <b>1</b>		24	76
7	pUC 19 + 30 $\mu\text{M}$ $\text{H}_2\text{O}_2$ + 30 $\mu\text{M}$ complex <b>2</b>		25	75

11), respectively, was observed. As the concentration of **1** and **2** was increased, the amount of NC (Form II) increased. At 20  $\mu\text{M}$  concentration of **2**, 72% NC (Form II) as well as 28% of linear form of DNA (Form III) were obtained, whereas in the case of **1** (20  $\mu\text{M}$ ), 56% NC (Form II) and 4% of linear form of DNA (Form III) obtained. When the concentrations of the complexes were increased to 30  $\mu\text{M}$ , the SC DNA was converted to 76% of NC, 24% of linear form by **1** and 75% of NC, 25% of linear form by **2**. At higher concentrations of **2** (20 and 30  $\mu\text{M}$ ), SC plasmid DNA is fully converted to linear forms (L) and the NC forms.

Both complexes show efficient nuclease activity in the presence of  $\text{H}_2\text{O}_2$ . The intense nuclease activities of **1** and **2** are apparently due to enhanced stabilization of Mo-peroxo species. This may be attributed to the fact that both complexes have diperoxo moiety which shows higher stability in  $\text{H}_2\text{O}_2$  and induces nicking to SC plasmid DNA. Based on their ability to convert the SC form (Form I) to the NC form (Form II) and linear form (Form III), it is observed that **2** shows higher ability to cleave the SC plasmid DNA when compared to that of **1**. This may be due to the fact that **2** with phenyl acetyl hydroxamic acid as ligand shows better interaction with DNA, as it can form better H-bond (vide docking study) compared to phenyl acetic acid ligand of **1**.

### 3.5. Molecular docking investigation on the interaction of DNA with **1** and **2**

The molecular docking technique is usually exploited to understand the drug–DNA interactions, which is essential for rational drug design and discovery. This also helps to establish the mechanism of action of the reactants by placing a small molecule into the binding site of the target specific region of DNA [34]. Different structural properties lead to different binding modes, whereby the molecular shape is a very important factor in determining the binding mode. The forces responsible for maintaining the stability of the DNA–intercalator complex include van der Waals forces, hydrogen bonding, hydrophobic charge transfer, and electrostatic complementarity. In our experiment, **1** and **2** were successively docked with the DNA duplex of the sequence d(CGCGAATTCGCG)2 dodecamer (PDB ID: 1BNA) in order

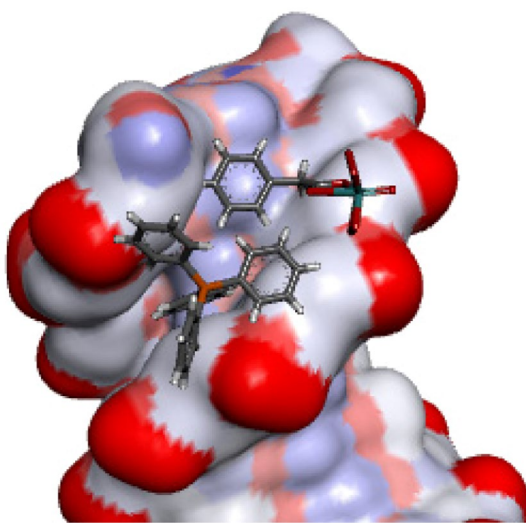


**Figure 12.** Docked pose of **1** showing interaction with base pairs.

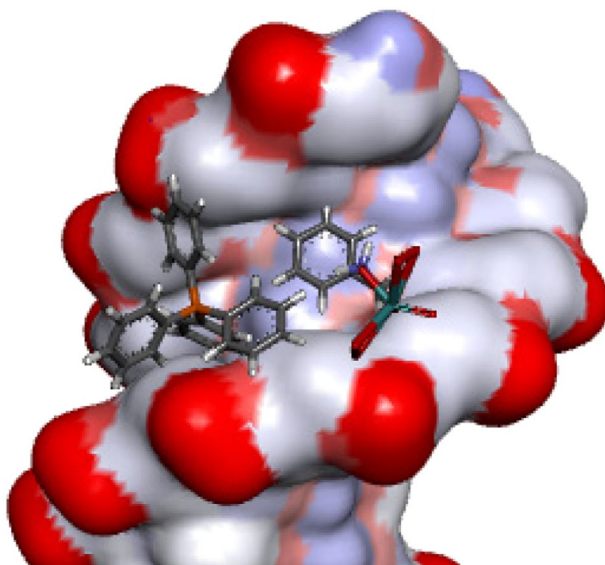


**Figure 13.** Docked pose of **2** showing interaction with base pairs.

to predict the chosen binding site along with preferred orientation of the ligand inside the DNA minor-groove [35]. The energetically most favorable conformation of the docked pose (Figures 12 and 13) revealed that **1** and **2** bind to DNA-groove, thereby slightly adjusting the DNA structure in such a way that part of the planar phenyl ring makes favorable stacking interactions with DNA base pairs through van der Waals interactions with the DNA functional groups which accounts for the stability of the groove. Moreover, two hydrogen bonding interactions with **2** in the minor groove have been predicted. The resulting relative binding energies of the docked structures for **1** and **2** were found to be  $-306.8 \text{ kJ mol}^{-1}$  and  $-298.78 \text{ kJ mol}^{-1}$ , respectively. This indicates potent binding between the DNA and both **1** and **2** which correlates well with the experimental DNA binding studies. Thus, the spectroscopic experimental results are harmonized with the molecular docking studies as well.

#### 4. Conclusion

Two oxo-peroxo molybdenum complexes are synthesized and characterized. Complex **1** is structurally characterized by single-crystal X-ray crystallography whereas **2** is optimized by DFT calculations and the TDDFT study also supports the optimized structure of **2** having an excellent agreement with the experimental findings. In the present study, the interaction of **1** and **2** with CT DNA is examined by absorbance and fluorescence spectroscopy, cyclic voltammetry and viscometric methods. The absorbance studies reveal that the intrinsic binding constant for **1** and **2** are  $5.2 \times 10^4$  and  $7.3 \times 10^4 \text{ M}^{-1}$ , respectively. The results suggest that **1** and **2** bind in the groove of CT DNA. This groove-binding nature of the complexes was further supported by cyclic voltammetry and viscosity study. Both complexes exhibit effective nuclease activity in the presence of  $\text{H}_2\text{O}_2$  by cleaving the supercoiled plasmid (pUC19) DNA to NC one. Complex **2** shows higher nuclease activity compared to **1**. At higher concentrations of **2**, SC form of DNA is completely converted to L and NC forms. The present

study reveals that the complexes may be used as a new class of rare non-platinum-based molybdenum nucleases.

## Electronic supplementary material

Crystallographic data for **1** (CCDC 1016513) are available as electronic supplementary information. These data can be obtained free of charge via <http://www.ccdc.cam.ac.uk/deposit> or from the Cambridge Crystallographic Data Center, 12 Union Road, Cambridge CB2 1EZ, UK; Fax: (+44) 1223–336-033; or E-mail: [deposit@ccdc.cam.ac.uk](mailto:deposit@ccdc.cam.ac.uk).

## Disclosure statement

No potential conflict of interest was reported by the authors.

## Funding

Authors are thankful to UGC, New Delhi for funding UVP Bio Doc-IT GEL Imaging system in the form of a major research project to Kalyan K. Mukherjea [grant number 39-706/2010(SR)]. Shiv Shankar Paul is thankful to UGC for fellowship. The single crystal X-ray diffractometer and NMR spectrometers used in this work have been funded by the Department of Science and Technology (DST-FIST, Department of Chemistry, J. U.), New Delhi, India.

## References

- [1] (a) P.C.A. Bruijninx, P.J. Sadler. *Curr. Opin. Chem. Biol.*, **12**, 197 (2008).; (b) A.C. Komor, J.K. Barton. *Chem. Commun.*, **49**, 3617 (2013); (c) L. Ronconi, P.J. Sadler. *Coord. Chem. Rev.*, **251**, 1633 (2007); (d) D. Wang, S.J. Lippard. *Nat. Rev. Drug Discov.*, **4**, 307 (2005).S. Gopal, (e) U.N. Balachandran. *Eur. J. Med. Chem.*, **45**, 284 (2010).
- [2] (a) V. Brabec, J. Malina, N. Margiotta, G. Natile. *Chem. Eur. J.*, **18**, 15439 (2012); (b) T.D. Tullius, J.A. Greenbaum. *Curr. Opin. Chem. Biol.*, **9**, 127 (2005); (c) J.D. West, L.J. Marnett. *Chem. Res. Toxicol.*, **19**, 173 (2006).
- [3] (a) W.K. Pogozelski, T.J. McNeese, T.D. Tullius. *J. Am. Chem. Soc.*, **117**, 6428 (1995).; (b) L.E. Pope, D.S. Sigman. *Proc. Natl. Acad. Sci. USA*, **81**, 3 (1984);(c) D.S. Sigman. *Biochemistry*, **29**, 9097 (1990); (d) M.P. Fitzsimmons, J.K. Barton. *J. Am. Chem. Soc.*, **119**, 3379 (1997); (e) A. Sreedhara, J.D. Freed, J.A. Cowan. *J. Am. Chem. Soc.*, **122**, 8814 (2000); (f) P. Ordoukhanian, G.F. Hoyce. *J. Am. Chem. Soc.*, **124**, 12499 (2002).
- [4] A. Radzicka, R. Wolfenden. *Science*, **267**, 90 (1995).
- [5] (a) M.E. Nunez, J.K. Barton. *Curr. Opin. Chem. Biol.*, **4**, 199 (2000).(b) S.E. Wolkenberg, D.L. Boger. *Chem. Rev.*, **102**, 2477 (2002).
- [6] M.A. Zenkova, N.G. Beloglazova, M.A. Zenkova. In *Nucleic Acids and Molecular Biology: Artificial Nucleases* (Ed.), **13**, 189 (2004).
- [7] (a) A. Ghosh, A. Mandoli, D.K. Kumar, N. Singh Yadav, T. Ghosh, B. Jha, J.A. Thomas. A. Das. *Dalton Trans.*, 9312, (2009).(b) M. Costas, M.P. Mehn, M.P. Jensen, L. Que Jr. *Chem. Rev.*, **104**, 939 (2004).(c) G. Parkin. *Chem. Rev.*, **104**, 699 (2004).(d) A.J. Wu, J.E. Penner-Hahn, V.L. Pecoraro. *Chem. Rev.*, **104**, 903 (2004).(e) D.C. Crans, J.J. Smee, E. Gaidamauskas, L. Yang. *Chem. Rev.*, **104**, 849 (2004).(f) L.M. Mirica, X. Ottenwaelder, T.D.P. Stack. *Chem. Rev.*, **104**, 1013 (2004).(g) W.K. Pogozelski, T.D. Tullius. *Chem. Rev.*, **98**, 1089 (1998).(h) C.J. Burrows, J.G. Muller. *Chem. Rev.*, **98**, 1109 (1998).(i) J. Qian, S. Yu, W. Wang, L. Wang, J. Tian, S. Yan. *Dalton Trans.*, **43**, 2646 (2014).
- [8] (a) G. Moula, M. Bose, S. Sarkar. *Inorg. Chem.*, **52**, 5316 (2013).(b) J. Mitra, S. Sarkar. *Dalton Trans.*, **42**, 3050 (2013).(c) A. Majumdar, S. Sarkar. *Coord. Chem. Rev.*, **255**, 1039 (2011).(d) P.K. Chaudhury, S.K. Das, S. Sarkar. *J. Biochem.*, **319**, 953 (1996).(e) S.K. Das, P.K. Chaudhury, D. Biswas, S. Sarkar.

- J. Am. Chem. Soc.*, **116**, 9061 (1994).(f) M. Sarma, T. Chatterjee, H. Vindhya, S.K. Das. *Dalton Trans.*, **41**, 1862 (2012).(g) B.E. Schultz, S.F. Gheller, M.C. Muetterties, M.J. Scott, R.H. Holm. *J. Am. Chem. Soc.*, **115**, 2714 (1993).
- [9] (a) M.L. Ramos, M.M. Calderia, V.M.S. Gil. *Dalton Trans.*, 2099, (2000).(b) B. Tamami, H. Yeganeh. *Eur. Polym. J.*, **35**, 1445 (1999).
- [10] (a) M. Komiyama, N. Takeda, H. Shigekawa. *Chem. Commun.*, 1443, (1999).(b) A. Sreedhara, J.A. Cowan. *J. Biol. Inorg. Chem.*, **6**, 337 (2001).(c) A. Kamal, R. Ramu, V. Tekumalla, G.B.R. Khanna, M.S. Barkume, A.S. Juvekar, S.M. Zingde. *Bioorg. Med. Chem.*, **15**, 6868 (2007).
- [11] (a) R. Eshkourfu, B. Cobeljic, M. Vujcic, I. Turel, A. Pevec, K. Sepcic, M. Zec, S. Radulovic, T. Srdic-Radic, D. Mitic, K. Andjelkovic, D. Sladic. *J. Inorg. Biochem.*, **105**, 1196 (2011).(b) A. Manna, S. Chakravorti. *J. Phys. Chem. B*, **116**, 5226 (2012).(c) N. Arshad, U. Yunus, S. Razzque, M. Khan, S. Saleem, B. Mirza, N. Rashid. *Eur. J. Med. Chem.*, **47**, 452 (2012).(d) R.F. Vitor, I. Correia, M. Videira, F. Marques, A. Paulo, J.C. Pessoa, G. Viola, G.G. Martins, I. Santos. *Chem. Bio. Chem.*, **9**, 131 (2008).
- [12] (a) N.H. Williams, B. Takasaki, M. Wall. *J. Chin. Acc. Chem. Res.*, **32**, 485 (1999).(b) B.D. Wang, Z.Y. Yang, P. Crewdson, D.Q. Wang. *J. Inorg. Biochem.*, **101**, 1492 (2007).(c) H. Xu, K.C. Zheng, Y. Chen, Y.Z. Li, L.J. Lin, H. Li, P.X. Zhang, L.N. Ji. *Dalton Trans.*, **11**, 2260 (2003).
- [13] S.S. Paul, M. Selim, A. Saha, K.K. Mukherjea. *Dalton Trans.*, **43**, 2835 (2014).
- [14] M. Selim, K.K. Mukherjea. *J. Biomol. Struct. Dyn.*, **26**, 561 (2009).
- [15] A.K. Majumdar. In *N-Benzoylphenyl Hydroxylamine and its Analogues*, R. Belcher, A. Frieser (Eds.), Pergamon Press, Braunschweig (1971).
- [16] Bruker, APEX 2, SAINT, XPREP, Bruker AXS Inc., Madison, WI (2007).
- [17] Bruker, SADABS, Bruker AXS Inc., Madison, WI (2001).
- [18] (a) SHELXS 97 and SHELXL 97, G.M. Sheldrick. *Acta Crystallogr., Sect. A: Found. Crystallogr.*, **64**, 112 (2008). (b) L.J. Farrugia. *J. Appl. Crystallogr.*, **30**, 565 (1997).
- [19] M.J. Frisch, G.W. Trucks, H.B. Schlegel, G.E. Scuseria, M.A. Robb, J.R. Cheeseman, G. Scalmani, V. Barone, B. Mennucci, G.A. Petersson, H. Nakatsuji, M. Caricato, X. Li, H.P. Hratchian, A.F. Izmaylov, J. Bloino, G. Zheng, J.L. Sonnenberg, M. Hada, M. Ehara, K. Toyota, R. Fukuda, J. Hasegawa, M. Ishida, T. Nakajima, Y. Honda, O. Kitao, H. Nakai, T. Vreven, J.A. Montgomery Jr, J.E. Peralta, F. Ogliaro, M. Bearpark, J.J. Heyd, E. Brothers, K.N. Kudin, V.N. Staroverov, R. Kobayashi, J. Normand, K. Raghavachari, A. Rendell, J.C. Burant, S.S. Iyengar, J. Tomasi, M. Cossi, N. Rega, J.M. Millam, M. Klene, J.E. Knox, J.B. Cross, V. Bakken, C. Adamo, J. Jaramillo, R. Gomperts, R.E. Stratmann, O. Yazyev, A.J. Austin, R. Cammi, C. Pomelli, J.W. Ochterski, R.L. Martin, K. Morokuma, V.G. Zakrzewski, G.A. Voth, P. Salvador, J.J. Dannenberg, S. Dapprich, A.D. Daniels, Ö. Farkas, J.B. Foresman, J.V. Ortiz, J. Cioslowski, D.J. Fox. Gaussian Inc., Wallingford, CT (2009).
- [20] (a) G.A. Paterson, M.A. Al-Laham. *J. Chem. Phys.*, **94**, 6081 (1991).(b) P.J. Hay, W.R. Wadt. *J. Chem. Phys.*, **82**, 270 (1985).(c) W.R. Wadt, P.J. Hay. *J. Chem. Phys.*, **82**, 284 (1985).(d) A.D. Becke. *J. Chem. Phys.*, **98**, 5648 (1993).(e) C. Lee, W. Yang, R.G. Parr. *Phys. Rev. B*, **37**, 785 (1988).
- [21] J. Mitra, S. Sarkar. *Inorg. Chem.*, **52**, 3032 (2013).
- [22] (a) S. Patra, S. Chatterjee, T.K. Si, K.K. Mukherjea. *Dalton Trans.*, **42**, 13425 (2013).(b) Y.M. Song, Q. Wu, P.J. Yang, N.N. Luan, L.F. Wang, Y.M. Liu. *J. Inorg. Biochem.*, **100**, 1685 (2006).(c) C. Tan, J. Liu, L. Chen, S. Shi, L. Ji. *J. Inorg. Biochem.*, **102**, 1644 (2008).(d) M.E. Reichmann, S.A. Rice, C.A. Thomas, P. Doty. *J. Am. Chem. Soc.*, **76**, 3047 (1954).(e) J. Marmur. *J. Mol. Biol.*, **3**, 208 (1961).
- [23] (a) T.K. Si, S.S. Paul, M.G.B. Drew, K.K. Mukherjea. *Dalton Trans.*, **41**, 5805 (2012).(b) A. Wolfe, G.H. Shimer, T. Meehan. *Biochemistry*, **26**, 6392 (1987).
- [24] J.B. Chaires, N. Dattagupta, D.M. Crothers. *Biochemistry*, **21**, 3933 (1982).
- [25] D. Mustard, D.W. Ritchie. *Protein Struct., Funct., Bioinf.*, **60**, 269 (2005).
- [26] (a) S.E. Jacobsen, R. Tang, F. Marcs. *Inorg. Chem.*, **17**, 3055 (1978).(b) N. Gharah, S. Chakraborty, A.K. Mukherjee, R.G. Bhattacharyya. *Inorg. Chim. Acta*, **362**, 1089 (2009).(c) R.D. Hancock, D.A. Thornton. *J. Mol. Struct.*, **6**, 441 (1970).(d) M.S. Islam, M.M. Uddin. *Polyhedron*, **11**, 2913 (1992).
- [27] (a) R. Bandyopadhyay, S. Biswas, S. Guha, A.K. Mukherjee, R. Bhattacharyya. *Chem. Commun.*, 1627, (1999).(b) R. Stomberg, S. Olson. *Acta Chem. Scand. Ser.*, **A39**, 79 (1985).
- [28] (a) K.R. Barnard, M. Bruck, S. Huber, C. Grittini, J.H. Enemark, R.W. Gable, A.G. Wedd. *Inorg. Chem.*, **36**, 637 (1997).(b) F. Han, N. Taulier, T.V. Chalikian. *Biochemistry*, **44**, 9785 (2005).(c) P.E. Pjura, K. Grzeskowiak, R.E. Dickerson. *J. Mol. Biol.*, **197**, 257 (1987).

- [29] (a) C. Behrens, N. Harrit, P.E. Nielsen. *Bioconjugate Chem.*, **12**, 1021 (2001).(b) S. Frau, J. Bernadou, B. Meunier. *Bioconjugate Chem.*, **8**, 222 (1997).(c) A.M. Pyle, J.P. Rehmann, R. Meshoyrer, C.V. Kumar, N.J. Turro, J.K. Barton. *J. Am. Chem. Soc.*, **111**, 3051 (1989).
- [30] (a) Y.C. Liu, Z.Y. Yang. *Eur. J. Med. Chem.*, **44**, 5080 (2009).(b) S. Satyanarayana, J.C. Dabrowiak, J.B. Chaires. *Biochemistry*, **32**, 2573 (1993).(c) D.S. Sigman, A. Mazumder, D.M. Perrin. *Chem. Rev.*, **93**, 2295 (1993).(d) Y. Wang, Z.-Y. Yang, Q. Wang, Q.-K. Cai, K.-B. Yu. *J. Organomet. Chem.*, **690**, 4557 (2005).(e) S. Satyanarayana, J.C. Dabrowiak, J.B. Chaires. *Biochemistry*, **31**, 9319 (1992).
- [31] (a) S.S. Zhang, S.Y. Niu, B. Qu, G.F. Jie, H. Xu, C.F. Ding. *J. Inorg. Biochem.*, **99**, 2340 (2005).(b) M.T. Carter, M. Rodriguez, A.J. Bard. *J. Am. Chem. Soc.*, **111**, 8901 (1989).
- [32] (a) A.J. Bard, L.R. Faulkner. *Electrochemical Methods*, Vol 219., Wiley, New York, NY (1980).(b) G. Psomas. *J. Inorg. Biochem.*, **102**, 1798 (2008).(c) K. Jiao, Q.X. Wang, W. Sun, F.F. Jian. *J. Inorg. Biochem.*, **99**, 1369 (2005).
- [33] (a) S. Ghosh, S.S. Paul, J. Mitra, K.K. Mukherjea. *J. Coord. Chem.*, **67**, 1809 (2014).(b) M. Selim, S.R. Choudhary, K.K. Mukherjea. *Int. J. Biol. Macromol.*, **41**, 579 (2007).(c) T.A. Dix, K.M. Hess, M.A. Medina, R.W. Sullivan, S.L. Tilly, T.L.L. Webb. *Biochemistry*, **35**, 4578 (1996).(d) T.H. Zastawny. *Free Rad, Biol. Med.*, **18**, 1013 (1995).(e) P. Tachon. *Free Rad. Res. Commun.*, **7**, 1 (1989).(f) P. Tachon. *Free Rad. Res. Commun.*, **9**, 39 (1990).(g) Q. Li, T.A. Berg, B.L. Feringa, G. Roelfes. *Dalton Trans.*, **39**, 8012 (2010).(h) T.A. Berg, B.L. Feringa, G. Roelfes. *Chem. Commun.*, **180**, (2007).(i) S. Gama, I. Rodrigues, F. Marques, E. Palma, I. Correia, M.F.N.N. Carvalho, J.C. Pessoa, A. Cruz, S. Mendo, I.C. Santos, F. Mendes, I. Santos, A. Paulo. *RSC Adv.*, **4**, 61363 (2014).(j) S. Gama, F. Mendes, F. Marques, I.C. Santos, M.F. Carvalho, I. Correia, J.C. Pessoa, I. Santos, A. Paulo. *J. Inorg. Biochem.*, **105**, 637 (2011).
- [34] (a) T.R. Li, Z.Y. Yang, B.D. Wang, D.D. Qin. *Eur. J. Med. Chem.*, **43**, 1688 (2008).(b) J.I. Ueda, N. Saito, Y. Shimazu, T. Ozawa. *Arch. Biochem. Biophys.*, **333**, 377 (1996).
- [35] (a) R. Rohs, I. Bloch, H. Sklenar, Z. Shakked. *Nucl. Acids Res.*, **33**, 7048 (2005).(b) R. Filosa, A. Peduto, S. Di Micco, P. de Caprariis, M. Festa, A. Petrella, G. Capranico, G. Bifulco. *Bioorg. Med. Chem.*, **17**, 13 (2009).(c) R. Corradini, S. Sforza, T. Tedeschi, R. Marchelli. *Chirality*, **19**, 269 (2007).(d) B.K. Sahoo, K.S. Ghosh, R. Bera, S. Dasgupta. *Chem. Phys.*, **351**, 163 (2008).(e) L.F. Pineda De Castro, M. Zacharias. *J. Mol. Recognit.*, **15**, 209 (2002).